CrystEngComm

Accepted Manuscript

ROYAL SOCIETY OF CHEMISTRY

www.rsc.org/crystengcomm

Gas-liquid segmented flow microwave-assisted synthesis of MOF-74(Ni) under moderate pressures

Gustavo H. Albuquerque,[1] Robert C. Fitzmorris,[1] Majid Ahmadi,[1] Nick Wannenmacher,[1] Praveen K. Thallapally,[2] B. Peter McGrail,[2] and Gregory S. Herman[1,*]

[1]Oregon State University, School of Chemical, Biological and Environmental Engineering, Corvallis, OR 97331-2702, USA

[2]Pacific Northwest National Laboratory, MSIN K4-18, Richland, WA 99352, USA

Corresponding Author

*E-mail: greg.herman@oregonstate.edu

Phone: 1-541-737-2496, Fax: 1-541-737-4600

TABLE OF CONTENTS ENTRY

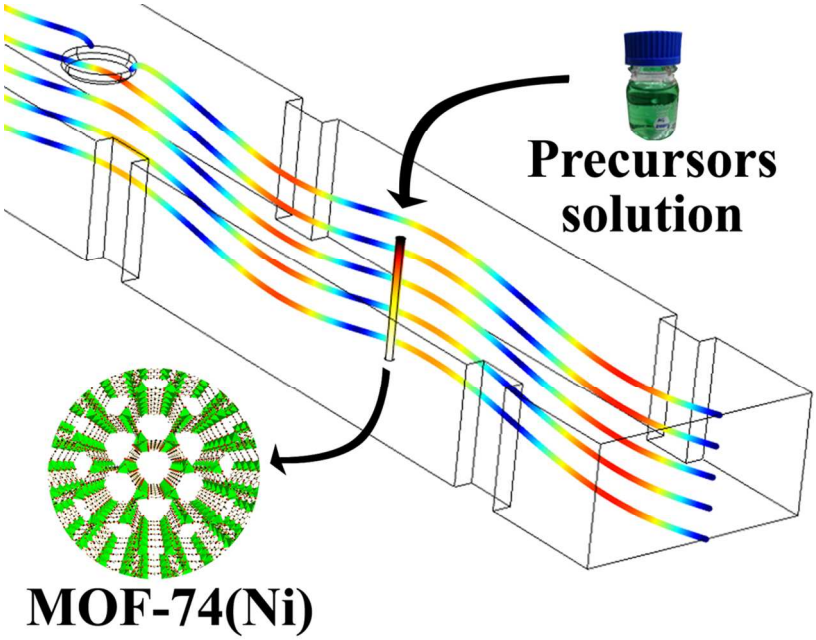

Representation of the continuous flow microwave-assisted synthesis of the metal organic framework, MOF-74(Ni). Nickel acetate and 2,5-dihydroxyterepthatic acid dissolved in dimethylformamide/deionized water flow through a microwave nucleation zone leading to formation of MOF-74(Ni).

ABSTRACT

The metal organic framework, MOF-74(Ni), was synthesized in a continuous flow microwave-assisted reactor obtaining high space-time yield (~90 $g.h^{-1}.L^{-1}$) and 96.5 % conversion of reagents. Separation o nucleation and growth steps was performed by using uniform and rapid microwave heating to induce nucleation, which allowed a substantial increase in conversion for shorter reaction times under mild pressure. High yields were achieved in minutes, as opposed to days for typical batch syntheses, with excellent control over material properties due to more uniform nucleation, and separation of the nucleation and growth steps. Optimization of microwave reactor parameters led to improvements in MOF-74(Ni) crystallinity, reagent conversion, and production rates. Differences in MOF-74(Ni) crystallinity were observed as smaller grains were formed when higher microwave zone temperatures were used. Crystallinity differences led to different final adsorption properties and surface areas. Herein we show that a continuous high space-time yield synthesis of MOF-74(Ni) allows control over nucleation using microwave heating.

Keywords: MOF-74(Ni), metal-organic frameworks (MOFs), microwave-assisted continuous flow synthesis

INTRODUCTION

Metal organic frameworks (MOFs) are of considerable scientific and technological interest due to their tunable porosity, high surface area, and the large number of available structures.[1–3] Metal ions coordinated with a wide variety of polytopic linkers (bridging ligands) form a crystalline nanoporous structure which provides advantages for applications including gas storage [4–10], gas separation [11–20], catalysis [21,22], sensing [23–25], and more recently pharmaceuticals.[26,27] The MOF-74 series, also known as CPO-27, (CPO = Coordination Polymer of Oslo) have high adsorption properties for carbon dioxide [12,15–17,28], noble gases [18,19], toxic gases [11,13], methane [29] and water[12,28,30]. MOF-74(Ni) is of increased interest for industrial applications due to the high relative stability in presence of moisture while maintaining high adsorption capacity even after many thermal adsorption/desorption cycles.[12,31]

MOFs provide many unique properties that can be tuned for distinct applications, however the lack of large-scale MOF synthesis methods that provide uniform high quality materials limits commercialization of many MOF enabled products. Traditional solvothermal syntheses of MOFs in batch reactors rely on long and energy intensive processes.[16,32,33] Alternative synthetic approaches have been developed to reduce expense and enhance processing to simultaneously provide better control over particle uniformity and growth by employing microfluidics[34,35], electrochemistry[36,37,38], sonochemistry, and microwave radiation.[20,39–42 ,43,44]

Scaling difficulties for MOFs have been overcome by employing continuous flow synthesis approaches using conventional heating or some of the previously mentioned methods.[45,46] These approaches make use of relatively high temperatures and pressures to keep the synthesis in the solvothermal regime which gives high yields.[37,47–49] Recently an efficient space-time production

approach has been published where a one-pot synthesis of the MOF-74(Ni) was carried out in water at atmospheric pressure with a 1 h reaction time.[50] This process generated 28.5 $g.h^{-1}.L^{-1}$ of product with 92 % yield. However, an even higher space-time yield may be possible by separating the nucleation and growth regimes during the synthesis process. Procedures such as hot injection have been employed to attain high concentrations of precursors above the nucleation temperature, which allows formation of uniform nuclei. This process is then followed by a lower temperature growth regime. This approach becomes very impractical for large volumes due to mass and heat transfer limitations that lead to formation of less uniform particles.[51]

Compared to conventional heating, microwave heating is an excellent approach for initiating nucleation because of the rapid heating rates and uniform volumetric heating which lead to instantaneous nucleation, homogeneous growth, and high reproducibility of reactions.[52,53] Microwave heating can lead to uniform formation of particles under milder temperature and pressure, with reaction times in minutes as opposed to hours or days. Excellent control over nanoparticle size with very narrow size distributions has been shown for reactions using microwave heating.[34,51,54,55] Further improvements have also been enabled by using gas-liquid segmented flow in combination with microwave heating due to improved mixing, which reduces particle fouling, and also leads to more reproducible results.[34,35,55]

In this study, a microwave-assisted continuous flow reactor using gas-liquid segmented flow was employed to induce fast nucleation to accelerate MOFs synthesis while facilitating control over particle size. Synthetic conditions for MOF-74(Ni), were optimized by varying both the nucleation zone (microwave reactor) and growth zone (heating bath) temperatures. Several parameters were varied with the objective of maximizing reagent conversion with the shortest

residence time under mild reaction conditions. The effect of microwave power and resulting nucleation temperature on the synthesis process was investigated to understand the underlying MOF formation mechanism.

RESULTS AND DISCUSSION

A schematic of the continuous flow microwave reactor is shown in Figure 1, where the nucleation and growth zones are indicated. The nucleation zone is heated using a microwave source, while the growth zone is heated using an oil bath. This system allows separation of the microwave zone temperature (T_{MW}), and the growth bath temperature (T_{GB}). Preliminary studies using single-phase flow were also performed to determine the effect of T_{MW} on conversion efficiencies when only using microwave zone with a nucleation time of ~1 second. For example, we observed formation of particles at T_{MW} = 70 °C (~4 % conversion) to 150 °C (~50 % conversion). Gas-liquid segmented flow was used to facilitate longer reaction times, and an inset in Figure 1 is provided which shows the velocity distribution in the liquid slugs. Gas-liquid segmented flow was also introduced to minimize fouling and deposition on reactor walls, which are common issues for continuous flow nanoparticle synthetic approaches. Deposition on the sidewall can cause clogging and also create hot spots in the microwave zone since deposited particles can have strong microwave absorption. Segmented flow has previously been employed in nanoparticle synthesis for inducing circulation within aqueous slugs and promoting better mass/heat transfer which results in more uniform products. [35,51,54]

Figure 2 shows powder X-ray diffraction (PXRD) data for particles synthesized using both the microwave zone and heating bath, as well as samples collected directly after the microwave

zone with no heating bath. The sample collected using T_{MW} = 70° C and T_{GB} = 120° C gave a PXRD pattern for MOF-74(Ni) which is in agreement with available crystallographic data.[5] The most intense peaks were observed at 2θ = 6.8° and 11.8° in all samples. The corresponding inter-planar spacings are d_{hkl} = 12.99 Å and 7.51 Å, which are associated to crystallographic planes (-120) and (030), respectively. Broad PXRD peaks were obtained for MOFs synthesized using only the microwave zone for T_{MW} between 70 to 150° C. The broad diffraction peaks could indicate formation of smaller particles or an amorphous phase. An increase in diffraction peak intensities were observed in the PXRD patterns for higher T_{MW}, which suggests the formation of more crystalline material as microwave power and nucleation temperature increase. However, addition of the growth bath appears to be necessary to prepare highly crystalline MOFs.

Raman spectroscopy was employed as a complementary technique to PXRD to investigate changes related to MOF-74(Ni) linker or linker-metal under different reaction conditions. Figure 3 shows Raman spectra for MOF-74(Ni) grown under the same conditions as the PXRD results shown in Figure 2. Assignments of the Raman peaks are based on prior results,[56] where peaks at 1619, 1560, 570 cm^{-1} are assigned to stretching vibrations and ring deformation vibrations from the benzene ring present in organic linker, respectively. Peaks at 1501 and 1416 cm^{-1} are assigned to $\upsilon(COO^-)_{asym}$ and $\upsilon(COO^-)_{sym}$, respectively. The very intense peak at 1275 cm^{-1} is assigned to υ(CO) species after deprotonation of the carboxylic acid groups. The peak at 827 cm^{-1} is assigned to benzene ring C-H bending modes and finally, the peak at 410 cm^{-1} is assigned to ($Ni\text{-}O_{ligand}$) bond vibration.[56]

All samples have similar relative peak intensities and peak widths for all T_{MW} using only the nucleation zone. This confirmed formation of MOF-74(Ni) for reactions run at both low and high T_{MW}. Based on the results of PXRD and Raman spectroscopy the T_{MW} changes the relative

crystallinity of MOF-74(Ni), where PXRD appears to be more sensitive to the long-range order of the MOF. Prior studies have shown differences in adsorption properties of MOF-74(Ni) samples that were synthesized in a microwave batch reactor.[20,20,41] In these prior studies, higher microwave powers led to formation of smaller particles due to higher nucleation rates in the presence of microwave radiation. The presence of smaller particles resulted in an enhancement of the adsorption capacity of N_2 and several hydrocarbons because of the higher surface area available.

In Figure 4 we show PXRD patterns for MOF-74(Ni) samples as a function of T_{MW}. For all samples T_{GB} remained constant at 130 °C with an 8 min residence time. From top to bottom the PXRD patterns correspond to no microwaves and T_{MW} = 70, 110, and 150 °C. In all cases the XRD patterns are consistent with what is expected for this materials system. There is a significant reduction in peak intensity when the T_{MW} was increased to 110 and 150 °C, suggesting a reduction in crystallinity. As shown in the inset, the highest intensity was observed for T_{MW} = 70 °C for the peak at 2θ = 31.7°. In Figure 5 we show Raman spectra for samples grown under identical conditions as in Figure 4. In all cases the Raman spectra were consistent with that expected for MOF-74(Ni) without any peak shifts. When T_{MW} was increased to 110 and 150 °C the Raman peaks became weaker and broader, where the highest intensities were observed for T_{MW} = 70 °C. These data suggest a general trend where there was a reduction of relative crystallinity for higher T_{MW}, with an optimal T_{MW} = 70 °C.

Raman and PXRD have limitations in the identification of structural defects that may be formed during the very fast nucleation induced in the MW zone, or by formation of smaller grains leading to a nanocrystalline material, or combination of both. As such, transmission electron microscopy (TEM) was used to investigate effects of T_{MW} and correlate to changes in

crystallinity. In Figure 6 A, B, and C we show TEM images for samples grown without microwave heating and with T_{MW} = 70 and 150 °C, respectively. Larger MOF grains were observed for samples synthesized without microwave heating, whereas T_{MW} = 150 °C showed formation of smaller agglomerated grains which was likely due to the high nucleation rates. Agglomeration and formation of nanocrystalline material at T_{MW} = 150 °C helps explain the increase in XRD and Raman peak widths. However, we found no major differences in PXRD, Raman, and TEM for samples synthesized at T_{MW} = 70 °C and the sample synthesized without microwave heating. Using TEM the distances between crystallographic planes (d_{hkl}) were estimated to be 1.30 nm and 0.78 nm, which are very close to the (-120) and (030) plane spacing in the MOF-74(Ni) structure. These plane spacing are also close to the values obtained from the PXRD data where 2θ = 6.8° and 11.8° correspond to d_{hkl} = 1.299 and 0.751 nm, respectively. The increase of relative crystallinity shown by PXRD and Raman spectroscopy for T_{MW} = 70 °C may be attributed to a balance between increased nucleation and reduction of both agglomeration and growth induced by fast reaction rates in microwave zone. Grain sizes for the synthesis at T_{MW} = 70 °C are larger in comparison to higher T_{MW} and comparable to grains in samples synthesized without microwave heating.

Particle size measurements were also compared for a range of T_{MW}. In Figure 7 we show that as T_{MW} increased the particle size increased and a broader particle size distribution was also observed. These results are summarized in Table 1. Higher nucleation rates should occur for the reactions run at higher T_{MW}, especially since T_{GB} remained constant, and should result in a reduction of particle size since formation of more nuclei in the microwave zone would lead to smaller particles after the growth bath. However, high T_{MW} could lead to growth with high rates of diffusion, which could lead to formation of non-uniform and agglomerated particles.

LaMer et al.[56] has described a model for nucleation and growth which illustrates the benefits of keeping these regimes separate. High, but still uniform, nucleation rates can be achieved when nucleation temperatures (i.e., T_{MW}) increase and can influence the final properties of particles since available precursor concentrations decrease rapidly while uniform nuclei are generated. However, the increase of nucleation temperatures also enhances diffusion and reaction rates. At higher nucleation temperatures rapid diffusion could influence the continuous growth of particles after fractions of a second in the microwave zone. Therefore, tuning the microwave reactor to achieve a regime in which significant nucleation occurs but diffusion and concentration are low enough to ensure slow and more uniform growth becomes a key factor to obtain more uniform particle synthesis.

The increase of nucleation rate as a function of T_{MW} could be confirmed by the increasing number of smaller grains observed on the sample synthesized at T_{MW} = 150 °C. However, this complex system, which was optimized for a high space-time-yield of MOF-74(Ni), has high reagent diffusion rates and increased mobility due to the high concentrations employed. Therefore, application of microwave energy that induced significant nucleation with a combination of less driven growth (T_{MW} = 70 °C) as opposed to highly driven growth (T_{MW} = 150 °C) resulted in larger grains and higher relative crystallinity. High T_{MW} does induced faster nucleation, but overheating results in new nuclei being formed due to high diffusion and mobility of precursors resulting in increased particle sizes. Increased broadening for the sample T_{MW} = 150 °C in the dynamic light scattering (DLS) results may indicate that growth and new nucleation occurred rather than isolated nucleation.

Another factor that could be considered as a plausible cause for agglomeration could be high microwave absorption by MOF-74(Ni). These particles could potential be hotspots and create

higher temperature gradients closer to their surface. Several experiments were performed by measuring the temperature of MOF-74(Ni) suspensions at different concentrations in the microwave zone. Initially we used a high absorbing solvent (deionized water and dimethylformamide (DMF) - 50 % v/v) containing different concentrations of MOFs (9.5, 4.75, and 1.9 $g.L^{-1}$) to evaluate their effect on T_{MW} at constant microwave power. None of the suspensions had significant temperature differences (± 2 °C) when compared to pure solvent. A second experiment was carried out using pure toluene (very low microwave absorbing solvent) and a suspension of MOFs containing 9.5 $g.L^{-1}$ of MOF-74(Ni). Again no significant differences in temperature were observed for the solvent compared to the suspensions.

In Figure 8 we show physisorption results for MOF-74(Ni) for different T_{MW}. For samples synthesized at T_{MW} = 70 °C, or without any microwave heating, the resulting N_2 physisorption isotherms were of type I (Brunauer classification) which is characteristic of microporous materials.[57] High T_{MW} changed the general behavior of measured isotherm to type 2, which is identified by an increase of N_2 uptake at high relative pressures. This change can be attributed to the agglomeration of the small crystals shown in Figure 6. In Figure 9 we show surface area measurements for the MOFs. High surface areas were obtained for all samples which were close to values available in the literature (1070 $m^2.g^{-1}$), even though the reactions in this study were significantly shorter.[32] An approximate pore diameter (d_p) of 11 Å was calculated for all samples using an incremental surface area analysis, which is in agreement with literature estimates for MOF-74(Ni).[12] However, a lower surface area and slightly shifted peak can be seen for the sample prepared at T_{MW} = 150 °C. In addition different intensities of cumulative surface area varying with T_{MW} was also observed, which may be related to the agglomerated grains obtained for this sample. These results also indicate that the total surface area for each sample differs as a

function T_{MW}. Pores and intracrystalline diffusion appear to be responsible for nearly all the area obtained by these measurements (d_p < 20 Å), although some contribution appears to occur in the region of 20 – 100 Å which could be attributed to regions in between agglomerated particles (intercrystalline diffusion).

The influence of different activation procedures and their relationship to the presence of pore collapse in MOFs has been previously studied.[59,60] For these studies interparticle mesoporosity was observed due to the misalignment of micropores at interparticle regions and grain boundaries. The presence of structural defects, with trapped solvent in the pores, can effect internal diffusion and therefore decrease total adsorption capacities. Therefore, the agglomeration seen in our samples could hinder intracrystalline diffusion due to grain/grain boundaries and consequently reduce available surface area for adsorption.

In Figure 10 we show thermogravimetric analysis data for MOF samples under flowing N_2. These data indicate that samples had mass losses associated to water and DMF desorption during the temperature ramp. The isothermal steps indicate steep weight losses that are correlated with desorption of moisture and residual solvents that remained in the pores after the activation process. The data also indicate that MOF-74(Ni) thermally decomposed at approximately 350 °C, which is consistent with prior studies.[50]

EXPERIMENTAL SECTION

Chemicals: All chemicals were used as purchased without any further purification. Nickel acetate tetrahydrate (> 98 %) was obtained from Alfa Aesar, 2,5-dihydroxyterepthalic acid (> 98 %), (DOBDC), was obtained from TCI America, and dimethylformamide (DMF) (99.8 %) was

obtained from EMD.

Synthesis: The continuous microwave-assisted synthesis of MOF-74(Ni) was performed at 2.5 bar under solvothermal conditions, where a second peristaltic pump was used as a back pressure regulator. The precursor solution was prepared by mixing 50 mL of nickel (II) acetate tetrahydrate (0.12 M) in deionized (DI) water with 50 mL DOBDC dissolved in DMF (0.06 M). Argon gas was injected into the system using a T-junction to attain segmented flow. The reaction system used Teflon® tubing (1/8 in. outer diameter, 1/16 in. inner diameter) in both the nucleation zone and growth bath. Precursors entered the nucleation zone that consisted of a microwave reactor with a waveguide (Sairem model PCCMWR340PVMR1PE GMP 30 K; 2.45 GHz; 3 kW) resulting in a nucleation residence time of ~ 1 second. The temperature in the microwave zone (T_{MW}) was measured using an infrared camera (FLIR model E40) that imaged a total irradiated length of approximately 4.7 cm. The growth region consisted of a 25.4 m long Teflon® coil submersed in an oil bath held at a fixed growth bath temperature (T_{GB}). The growth region had an average residence time of about 8 min. After the reaction a liquid dispersion of the product was collected in a glass vial and then centrifuged to separate particles from solvents and unconverted reagents. MOF particles were then treated in the purification step by adding approximately 10 mL of water, followed by a second centrifugation with an addition of 10 mL of methanol. Over three days the particles were centrifuged and washed in 10 mL of fresh methanol up to four times. Activation was performed by keeping the samples under vacuum at 80 °C for three days prior to characterization.

Characterization: Powder X-ray diffraction (PXRD) was performed at room temperature using a Rigaku Ultima IV diffractometer (Cu-Kα = 0.1542 nm). Data was collected from 2θ = 5-50°. Prior to PXRD, the dried powder was ground for about 2 min using a mortar and pestle. All

PXRD were obtained on the same day, with no changes in the instrumental experimental conditions, so direct quantitative analysis could be made between spectra. Thermogravimetric analysis (TGA) was performed using a TA Instruments TGA Q500. Samples were exposed to air for about 30 min and then heated up to 600 °C using a 10 °C/min ramp rate with a N_2 flow rate of 60 mL/min. Two isothermal steps were taken at 105 and 250 °C for 20 min each. Transmission electron microscopy (TEM) imaging was performed using a FEI Titan FEG at 200 kV. For TEM imaging, samples were prepared from a hexane dispersion of MOF-74(Ni) particles, which was sonicated for 10 min prior to preparation (Branson model 2510 – Max power 130 W). A carbon coated copper grid was dipped into the MOF dispersion twice and mounted in the microscope after drying at room temperature. Scanning electron microscopy (SEM) imaging was performed using an FEI Quanta 600 FEG SEM with 15-30 kV accelerating voltage. Raman spectra were obtained using a Horiba-Jobin Yvon HR-800 Raman spectrometer with a 532 nm incident laser source. UV-Vis spectroscopy was performed using an AvaSpec-3648 spectrometer on the precursor solution and the supernatant obtained from centrifuged reaction products to estimate conversion efficiencies. N_2 physisorption measurements were obtained using a Micromeritics ASAP 2020. Particle size was determined using dynamic light scattering (DLS) on a Brookhaven Instruments Corp. Zeta Potential analyzer. For the DLS measurements MOF-74(Ni) suspensions (in hexane) were analyzed after 30 min of sonication.

CONCLUSIONS

In summary, a continuous and segmented flow microwave-assisted synthesis of the MOF-74(Ni) was performed under mild conditions of pressure (~2.5 bar) with high conversion of

reagents (~ 96.5 %) and space-time yield (~ 80 – 90 $g.h^{-1}.L^{-1}$). Segmented flow was employed to improve mixing and reduce particle fouling which allowed long reactions to be run with very good reproducibility of results. Very stable T_{MW} were obtained in the segmented flow regime for all reactions reported. The microwave zone helped reduce reaction times down to 8 min and increased nucleation. Faster nucleation at higher T_{MW} resulted in the formation of smaller grains, which resulted in different adsorption behavior even after the growth bath. This was due an agglomeration of grains and formation of structural defects at higher T_{MW}, and may result in misaligned and collapsed pores. High microwave absorption by solvents and higher diffusion conditions could significant influence growth in microwave zone and possibly result in more heterogeneous particles.

ACKNOWLEDGEMENTS

This work was funded by the United States Department of Energy through ARPA-e and the Department of the Navy.

REFERENCES

1 R. J. Kuppler, D. J. Timmons, Q.-R. Fang, J.-R. Li, T. A. Makal, M. D. Young, D. Yuan, D. Zhao, W. Zhuang and H.-C. Zhou, *Coord. Chem. Rev.*, 2009, **253**, 3042–3066.

2 N. L. Rosi, J. Kim, M. Eddaoudi, B. Chen, M. O'Keeffe and O. M. Yaghi, *J. Am. Chem. Soc.*, 2005, **127**, 1504–1518.

3 H. Furukawa, K. E. Cordova, M. O'Keeffe and O. M. Yaghi, *Science*, 2013, **341**, 1230444–1230444.

4 P. D. C. Dietzel, P. A. Georgiev, J. Eckert, R. Blom, T. Strässle and T. Unruh, *Chem. Commun.*, 2010, **46**, 4962.

5 M. T. Kapelewski, S. J. Geier, M. R. Hudson, D. Stück, J. A. Mason, J. N. Nelson, D. J. Xiao, Z. Hulvey, E. Gilmour, S. A. FitzGerald, M. Head-Gordon, C. M. Brown and J. R. Long, *J. Am. Chem. Soc.*, 2014, **136**, 12119–12129.

6 S. S. Kaye, A. Dailly, O. M. Yaghi and J. R. Long, *J. Am. Chem. Soc.*, 2007, **129**, 14176–14177.

7 A. R. Millward and O. M. Yaghi, *J. Am. Chem. Soc.*, 2005, **127**, 17998–17999.

8 R. Plessius, R. Kromhout, A. L. D. Ramos, M. Ferbinteanu, M. C. Mittelmeijer-Hazeleger, R. Krishna, G. Rothenberg and S. Tanase, *Chem. - Eur. J.*, 2014, **20**, 7922–7925.

9 N. L. Rosi, *Science*, 2003, **300**, 1127–1129.

10 D. Saha, R. Zacharia, L. Lafi, D. Cossement and R. Chahine, *Int. J. Hydrog. Energy*, 2012, **37**, 5100–5107.

11 S. Chavan, F. Bonino, L. Valenzano, B. Civalleri, C. Lamberti, N. Acerbi, J. H. Cavka, M. Leistner and S. Bordiga, *J. Phys. Chem. C*, 2013, **117**, 15615–15622.

12 A. Das, P. D. Southon, M. Zhao, C. J. Kepert, A. T. Harris and D. M. D'Alessandro, *Dalton Trans.*, 2012, **41**, 11739.

13 T. Grant Glover, G. W. Peterson, B. J. Schindler, D. Britt and O. Yaghi, *Chem. Eng. Sci.*, 2011, **66**, 163–170.

14 Z. R. Herm, E. D. Bloch and J. R. Long, *Chem. Mater.*, 2014, **26**, 323–338.

15 P. Kanoo, A. C. Ghosh, S. T. Cyriac and T. K. Maji, *Chem. - Eur. J.*, 2012, **18**, 237–244.

16 J. Liu, J. Tian, P. K. Thallapally and B. P. McGrail, *J. Phys. Chem. C*, 2012, **116**, 9575–9581.

17 Q. Liu, L. Ning, S. Zheng, M. Tao, Y. Shi and Y. He, *Sci. Rep.*, 2013, **3**.

18 J. J. Perry, S. L. Teich-McGoldrick, S. T. Meek, J. A. Greathouse, M. Haranczyk and M. D. Allendorf, *J. Phys. Chem. C*, 2014, **118**, 11685–11698.

19 P. K. Thallapally, J. W. Grate and R. K. Motkuri, *Chem. Commun.*, 2012, **48**, 347.

20 X. Wu, Z. Bao, B. Yuan, J. Wang, Y. Sun, H. Luo and S. Deng, *Microporous Mesoporous Mater.*, 2013, **180**, 114–122.

21 J. Liu, L. Chen, H. Cui, J. Zhang, L. Zhang and C.-Y. Su, *Chem Soc Rev*, 2014, **43**, 6011–6061.

22 J. Lee, O. K. Farha, J. Roberts, K. A. Scheidt, S. T. Nguyen and J. T. Hupp, *Chem. Soc. Rev.*, 2009, **38**, 1450.

23 L. E. Kreno, K. Leong, O. K. Farha, M. Allendorf, R. P. Van Duyne and J. T. Hupp, *Chem. Rev.*, 2012, **112**, 1105–1125.

24 S. Achmann, G. Hagen, J. Kita, I. M. Malkowsky, C. Kiener and R. Moos, *Sensors*, 2009, **9**, 1574–1589.

25 S. Zhang, L. Han, L. Li, J. Cheng, D. Yuan and J. Luo, *Cryst. Growth Des.*, 2013, **13**, 5466–5472.

26 S. Rojas, P. S. Wheatley, E. Quartapelle-Procopio, B. Gil, B. Marszalek, R. E. Morris and E. Barea, *CrystEngComm*, 2013, **15**, 9364.

27 P. Horcajada, T. Chalati, C. Serre, B. Gillet, C. Sebrie, T. Baati, J. F. Eubank, D. Heurtaux, P. Clayette, C. Kreuz, J.-S. Chang, Y. K. Hwang, V. Marsaud, P.-N. Bories, L. Cynober, S. Gil, G. Férey, P. Couvreur and R. Gref, *Nat. Mater.*, 2010, **9**, 172–178.

28 J. Liu, Y. Wang, A. I. Benin, P. Jakubczak, R. R. Willis and M. D. LeVan, *Langmuir*, 2010, **26**, 14301–14307.

29 J. A. Mason, M. Veenstra and J. R. Long, *Chem. Sci.*, 2014, **5**, 32.

30 P. M. Schoenecker, C. G. Carson, H. Jasuja, C. J. J. Flemming and K. S. Walton, *Ind. Eng. Chem. Res.*, 2012, **51**, 6513–6519.

31 J. Liu, A. I. Benin, A. M. B. Furtado, P. Jakubczak, R. R. Willis and M. D. LeVan, *Langmuir*, 2011, **27**, 11451–11456.

32 S. R. Caskey, A. G. Wong-Foy and A. J. Matzger, *J. Am. Chem. Soc.*, 2008, **130**, 10870–10871.

33 P. D. C. Dietzel, B. Panella, M. Hirscher, R. Blom and H. Fjellvåg, *Chem. Commun.*, 2006, 959.

34 L. Paseta, B. Seoane, D. Julve, V. Sebastián, C. Téllez and J. Coronas, *ACS Appl. Mater. Interfaces*, 2013, **5**, 9405–9410.

35 M. Faustini, J. Kim, G.-Y. Jeong, J. Y. Kim, H. R. Moon, W.-S. Ahn and D.-P. Kim, *J. Am. Chem. Soc.*, 2013, **135**, 14619–14626.

36 M. Li and M. Dincă, *J. Am. Chem. Soc.*, 2011, **133**, 12926–12929.

37 N. Campagnol, T. Van Assche, T. Boudewijns, J. Denayer, K. Binnemans, D. De Vos and J. Fransaer, *J. Mater. Chem. A*, 2013, **1**, 5827.

38 2007/0227898 A1, 2007.

39 J.-S. Lee, S. B. Halligudi, N.-H. Jang, D.-W. Hwang, J.-S. Chang and Y.-K. Hwang, *Bull. Korean Chem. Soc.*, 2010, **31**, 1489–1495.

40 E. Haque, N. A. Khan, J. H. Park and S. H. Jhung, *Chem. - Eur. J.*, 2010, **16**, 1046–1052.

41 E. Haque and S. H. Jhung, *Chem. Eng. J.*, 2011, **173**, 866–872.

42 N. A. Khan and S. H. Jhung, *Coord. Chem. Rev.*, 2015, **285**, 11-23.

43 J. Ren, T. Segakweng, H. W. Langmi, N. M. Musyoka, B. C. North, M. Mathe and D. Bessarabov, *Int. J. Mater. Res.*, 2014, **105**, 516–519.

44 C.-M. Lu, J. Liu, K. Xiao and A. T. Harris, *Chem. Eng. J.*, 2010, **156**, 465–470.

45 K.-J. Kim, Y. J. Li, P. B. Kreider, C.-H. Chang, N. Wannenmacher, P. K. Thallapally and H.-G. Ahn, *Chem. Commun.*, 2013, **49**, 11518.

46 P. M. Schoenecker, G. A. Belancik, B. E. Grabicka and K. S. Walton, *AIChE J.*, 2013, **59**, 1255–1262.

47 P. A. Bayliss, I. A. Ibarra, E. Pérez, S. Yang, C. C. Tang, M. Poliakoff and M. Schröder, *Green Chem.*, 2014, **16**, 3796.

48 M. Rubio-Martinez, M. P. Batten, A. Polyzos, K.-C. Carey, J. I. Mardel, K.-S. Lim and M. R. Hill, *Sci. Rep.*, 2014, **4**.

49 M. Gimeno-Fabra, A. S. Munn, L. A. Stevens, T. C. Drage, D. M. Grant, R. J. Kashtiban, J. Sloan, E. Lester and R. I. Walton, *Chem. Commun.*, 2012, **48**, 10642.

50 S. Cadot, L. Veyre, D. Luneau, D. Farrusseng and E. Alessandra Quadrelli, *J Mater Chem A*, 2014, **2**, 17757–17763.

51 K.-J. Kim, R. P. Oleksak, E. B. Hostetler, D. A. Peterson, P. Chandran, D. M. Schut, B. K. Paul, G. S. Herman and C.-H. Chang, *Cryst. Growth Des.*, 2014, **14**, 5349–5355.

52 S. Horikoshi and N. Serpone, *Microwaves in Nanoparticle Synthesis: Fundamentals and Applications*, Wiley-VCH, 2013.

53 R. P. Oleksak, B. T. Flynn, D. M. Schut and G. S. Herman, *Phys. Status Solidi A*, 2014, **211**, 219–225.

54 E. B. Hostetler, K.-J. Kim, R. P. Oleksak, R. C. Fitzmorris, D. A. Peterson, P. Chandran, C.-H. Chang, B. K. Paul, D. M. Schut and G. S. Herman, *Mater. Lett.*, 2014, **128**, 54–59.

55 V. Sebastian Cabeza, S. Kuhn, A. A. Kulkarni and K. F. Jensen, *Langmuir*, 2012, **28**, 7007–7013.

56 V. K. LaMer and R. H. Dinegar, *J. Am. Chem. Soc.*, 1950, **72**, 4847–4854.

57 S. Brunauer, L. S. Deming, W. E. Deming and E. Teller, *J. Am. Chem. Soc.*, 1940, **62**, 1723–1732.

58 A. P. Nelson, O. K. Farha, K. L. Mulfort and J. T. Hupp, *J. Am. Chem. Soc.*, 2009, **131**, 458–460.

59 C.-S. Tsao, C.-Y. Chen, T.-Y. Chung, C.-J. Su, C.-H. Su, H.-L. Chen, U.-S. Jeng, M.-S. Yu, P.-Y. Liao, K.-F. Lin and Y.-R. Tzeng, *J. Phys. Chem. C*, 2010, **114**, 7014–7020.

TABLES

Table 1: Particle size obtained from dynamic light scattering and scanning electron microscope. Particles were measured using software ImageJ®.

Conditions	**$d_{p\text{ - DLS}}$ (nm)**	**$d_{p\text{ - SEM}}$ (nm)**
No MW	1483 ± 140	1200 ± 430
MW 70 °C	1557 ± 142	1333 ± 470
MW 150 °C	2505 ± 170	2240 ± 1110

Table 2: Reagents conversion (evaluated using UV-Vis spectroscopy for Ni^{+2} concentration), mass production rate of MOF-74(Ni), and XRD full width at half maximum (FWHM) from reactions operated in segmented flow at different T_{MW}.

Conditions	**Conversion (%)**	**Mass prod. rate MOF-74(Ni) (g/h)**	**XRD FWHM at 31.75° (°)**	**S_{BET} (m^2/g)**
No MW	90.8	3.93	0.660	1012 ± 6
MW 70 °C	92.3	4.46	0.536	938 ± 6
MW 110 °C	94.3	4.51	0.662	936 ± 6
MW 150 °C	96.5	4.56	0.850	840 ± 3

FIGURE CAPTIONS

Figure 1: Schematic of segmented continuous flow microwave-assisted synthetic reactor for MOF-74(Ni). Model on top right was obtained using Comsol® shows turbulence in between slugs in segmented flow.

Figure 2: XRD data from MOF-74(Ni) synthesized at different T_{MW} compared to a sample, which has been synthesized using a combination of both microwave zone and growth zone. (Peak at $2\theta = 44$ ° present in samples from microwave only synthesis is due to XRD metal sample stage)

Figure 3: Raman spectra of MOF-74(Ni) samples, which were synthesized at different T_{MW} compared to a sample that went through a combination of microwave zone and growth zone.

Figure 4: XRD data of samples synthesized at different T_{MW} while growth zone was maintained at constant temperature and residence time. (XRD peaks at 31.75 ° are shown in inset)

Figure 5: Raman spectroscopy of MOF-74(Ni) samples synthesized at different T_{MW} while growth zone was maintained at constant temperature and residence time.

Figure 6: TEM images of samples synthesized without microwaves (A) and at T_{MW} = 70 and 150 °C (B and C, respectively).

Figure 7: Particle size measurements using on dynamic light scattering taken for samples synthesized with and without microwaves, and different T_{MW}.

Figure 8: N_2 physisorption isotherms obtained for segmented continuous flow synthesis of MOF-74(Ni) with and without the use of microwaves. T_{MW} was also varied keeping the

average residence time constant (0.93 s) while growth zone conditions were fixed at 130 °C for 8 min.

Figure 9: Cumulative surface area (solid lines) and Incremental surface area (crosses) for MOF-74(Ni) synthesized using segmented flow with and without the use of microwaves. T_{MW} was also varied keeping the average residence time constant (0.93 s) while heating zone conditions were fixed at 130 °C for 8 min.

Figure 10: Thermographic analysis performed on MOF-74(Ni) samples synthesized with and without microwaves, and at two different T_{MW}.

Figure 1

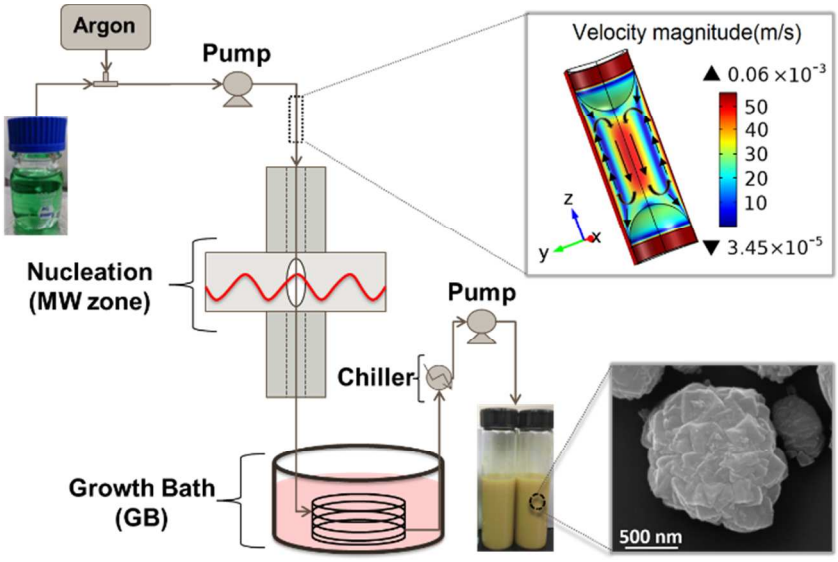

Figure 2

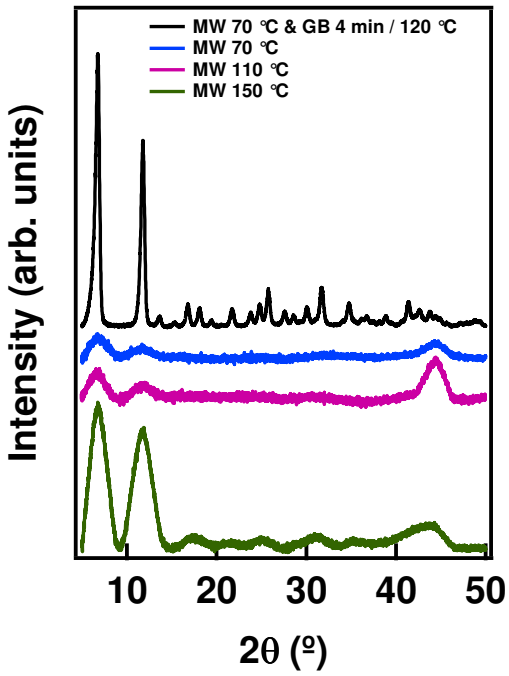

Figure 3

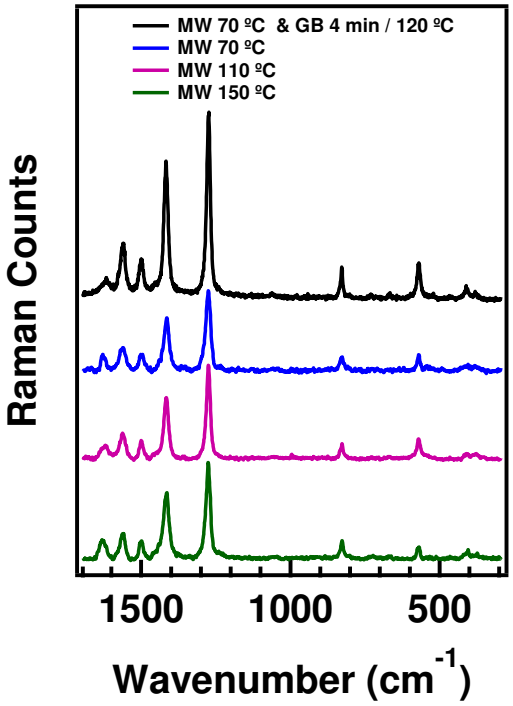

Figure 4

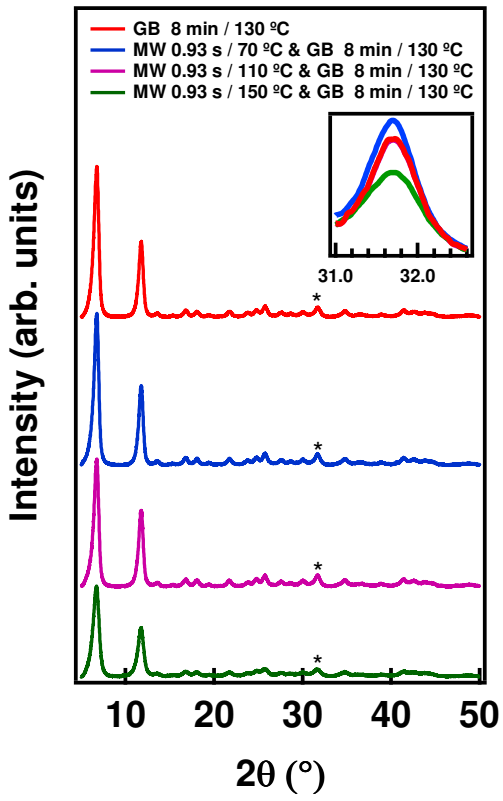

Figure 5

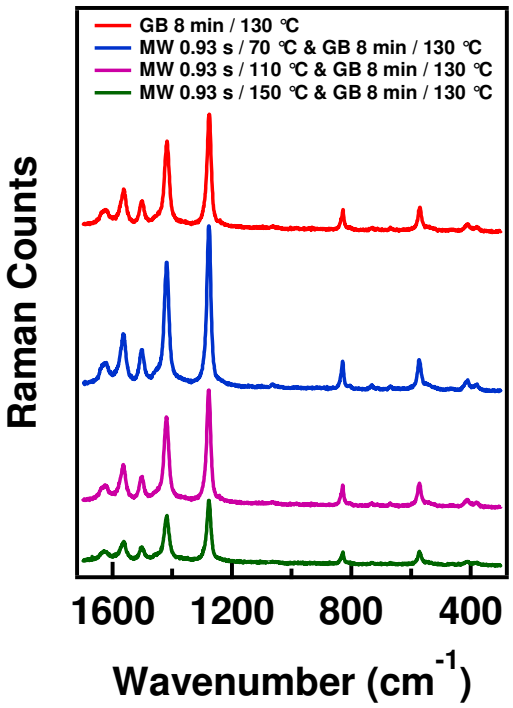

Figure 6

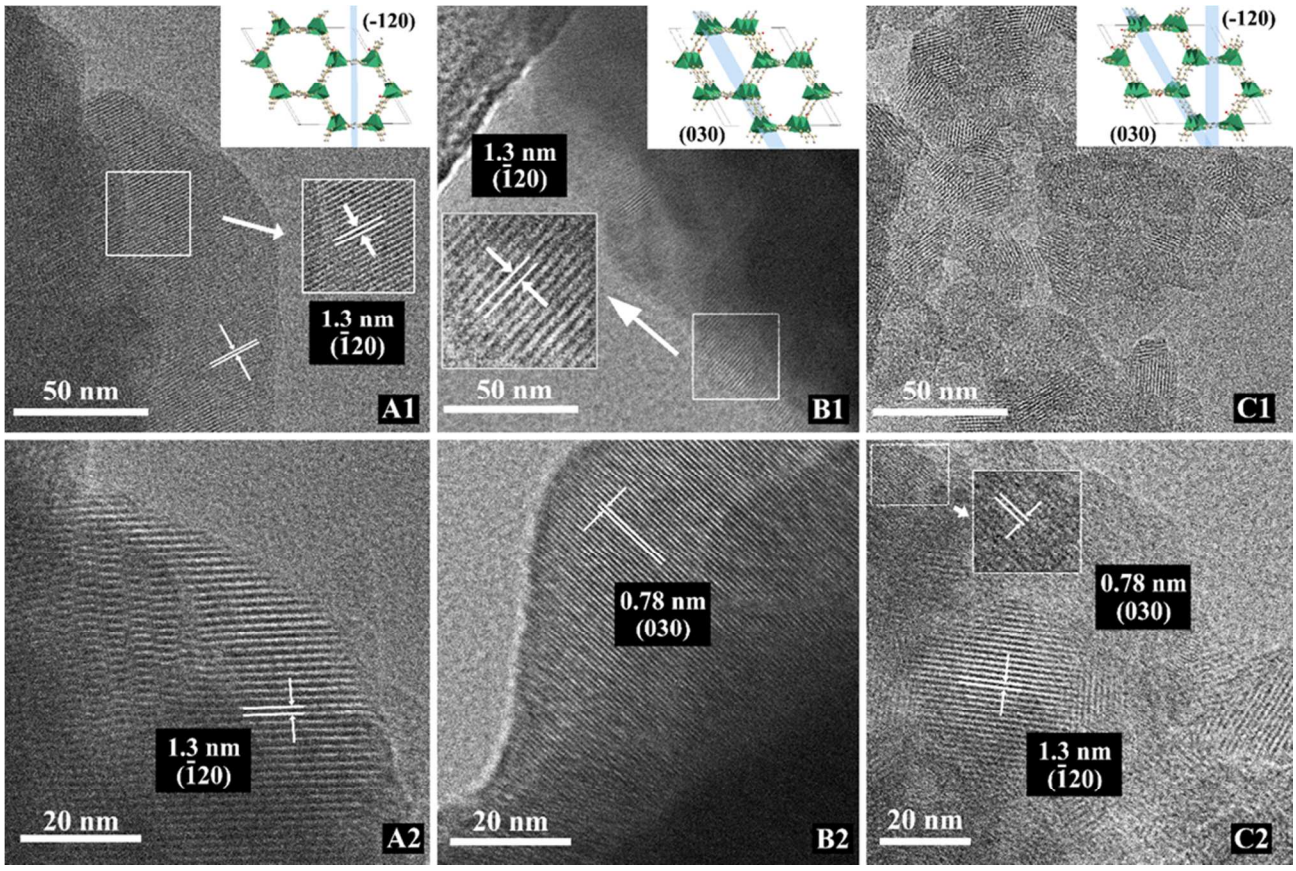

Figure 7

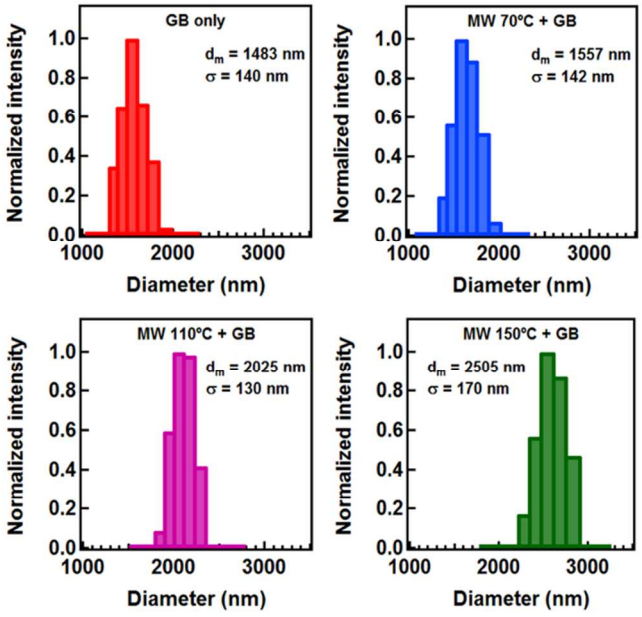

Figure 8

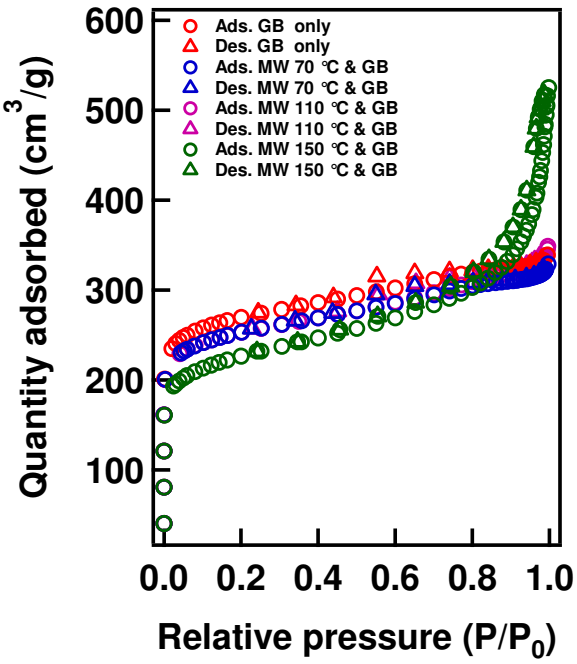

Figure 9

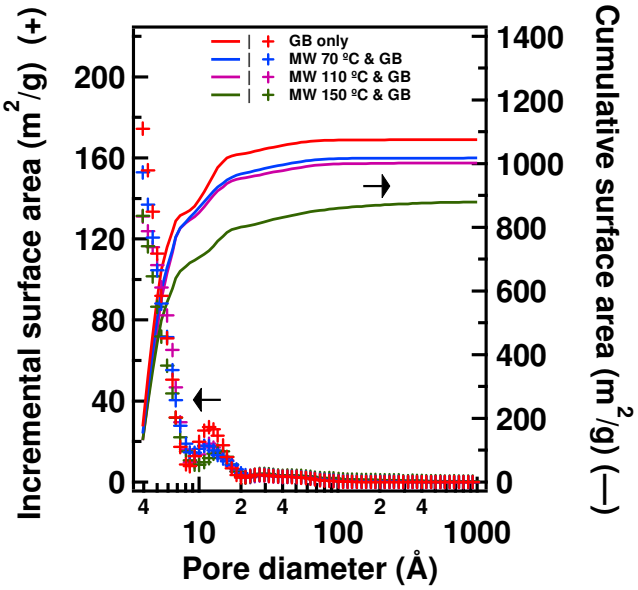

Figure 10